Kinetic Study of CH_3 + HBr and CH_3 + Br Reactions by Laser Photolysis−Transient Absorption over 1−100 Bar Pressure Range

Lev N. Krasnoperov* and Kashyap Mehta†

Department of Chemical Engineering, Chemistry and Environmental Science, New Jersey Institute of Technology, University Heights, Newark, New Jersey 07102

Received: April 8, 1999; In Final Form: August 6, 1999

Reactions of methyl radicals with hydrogen bromide $CH_3 + HBr \rightarrow CH_4 + Br$ (1) and bromine atoms $CH_3 + Br \rightarrow CH_3Br$ (2) were studied using excimer laser photolysis−transient UV spectroscopy at 297 ± 3 K over the 1−100 bar buffer gas (He) pressure range. Methyl radicals were produced by 193 nm (ArF) laser photolysis of acetone, $(CH_3)_2CO$, and methyl bromide, CH_3Br. Temporal profiles of methyl radicals were monitored by UV absorption at 216.51 nm (copper hollow cathode lamp with current boosting). The yield of acetyl radicals in photolysis of acetone at 193 nm was found to be less than 5% at 100 bar He based on the transient absorptions at 222.57 and 224.42 nm. The measured rate constants for reaction 1 are $k_1 = (2.9 \pm 0.7) \times 10^{-12}$, $(3.8 \pm 1.5) \times 10^{-12}$, and $(3.4 \pm 1.3) \times 10^{-12}$ cm^3 molecule^{-1} s^{-1} at the buffer gas (He) pressures of 1.05, 11.2, and 101 bar, respectively. The rate data obtained in this study confirmed high values of the previous (low pressure) measurements and ruled out the possibility of interference of excited species. The measured rate constant is independent of pressure within the experimental error. The rate constant of reaction of methyl radicals with bromine atoms (2) was determined relative to the rate constant of methyl radical self-reaction, $CH_3 + CH_3 \rightarrow C_2H_6$ (3) in experiments with photolysis of CH_3Br: $k_2/k_3 = 0.92 \pm 0.32$, 1.15 ± 0.30, and 1.65 ± 0.26 at 1.05, 11.2, and 101 bar He, respectively. On the basis of the literature data for reaction 3, this yields $k_2 = (5.8 \pm 2.2) \times 10^{-11}$, $(7.4 \pm 2.2) \times 10^{-11}$, $(10.7 \pm 2.3) \times 10^{-11}$, and $(11.9 \pm 2.5) \times 10^{-11}$ cm^3 molecule^{-1} s^{-1} at 1.05, 11.2, 101 bar (He), and in the high-pressure limit, respectively.

Introduction

Reactions of small hydrocarbon free radicals (such as CH_3, C_2H_5, C_3H_7, C_4H_9) with hydrogen halides (HI, HBr, and HCl) have been a subject of research during the last 50 years.[1−22] Beyond their importance for the fundamental chemical kinetics, these kinetic measurements were used as a source of the C−H bond energies.[22] Combination of the rate constant of reaction of a free radical with hydrogen halide with the rate constant of the reverse reaction, reaction of the halogen atom with the corresponding hydrocarbon molecule, yields a temperature-dependent equilibrium constant. Equilibrium constant data provide the standard enthalpy and entropy of the reaction using the second and the third laws.[22] Being combined with the accurately known thermodynamic properties of other reactants and products of reaction (of hydrogen halide, halogen atom, and the hydrocarbon molecule), these data allow accurate determination of the C−H bond energies in hydrocarbon molecules and the enthalpies of formation of free radicals.[22]

Recent theoretical and experimental kinetic studies performed using a variety of experimental techniques revealed negative apparent activation energies for reactions of small hydrocarbon free radicals with HI and HBr.[7,9,10,12−19,21] These observations lead to a substantial re-evaluation of C−H bond energies in small hydrocarbon molecules.[12−19,21] A possible explanation of the negative temperature dependence was given in terms of a "well" in the potential energy surface which corresponds to a bound complex and in terms of "chemically activated" system treatment.[20,23−25] A shallow well was indeed found in ab initio calculations.[20,24] The RRKM calculation with the theoretical potential energy surface with an adjusted "transition state" energy confirmed the possibility of negative activation energies which were experimentally observed.[20,24]

The results of these direct studies are in considerable discrepancy with the data obtained using the very low pressure reactor (VLPR) technique, both in the absolute values of the rate constants and in their temperature dependencies.[26−28] The VLPR studies (which are based on the measurement of the steady-state concentrations of the reaction species in a Knudsen cell), resulted in much lower rate constants and in positive activation energies. For example, for the reaction of t-C_4H_9 + DBr, the ambient temperature VLPR rate constant is 144 times lower than the one measured using laser pulsed photolysis.[18,26] Significant discrepancy was observed for the reaction of ethyl radicals with HBr; the reported rate constant at 298 is 14 times lower than that measured in the time-resolved studies.[21,27]

The whole series of the direct measurements which lead to negative activation energies and high rate constants in reactions of small hydrocarbon free radicals with HBr and HI was recently criticized.[27,28] The main point of this criticism is in the possible presence and interference of highly vibrationally excited free radicals after pulsed photolysis of the radical precursor molecules, used in all direct studies, which allegedly lead to negative values of the activation energies due to the interference of excited species.

In view of the tremendous importance of this issue for the thermochemistry of hydrocarbon free radicals and for the kinetics of simple metathesis reactions, one of the simplest reactions of this class, the reaction of methyl radicals with

* To whom correspondence should be addressed. E-mail: KRASNOPEROV@ADM.NJIT.EDU.

† Undergraduate summer research student, 1996.

10.1021/jp991183i CCC: $18.00
Published on Web 09/16/1999

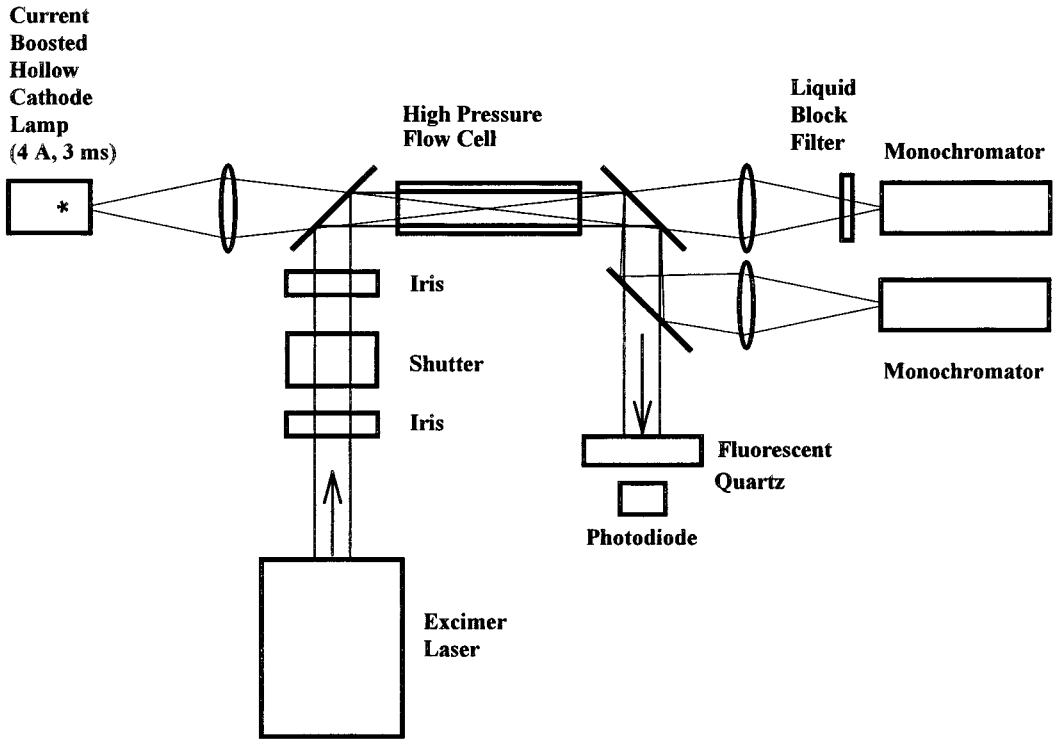

Figure 1. Experimental setup. Pulsed laser photolysis coupled to a UV−vis transient absorption spectroscopy.

hydrogen bromide (1), was reinvestigated in the current work over an extended buffer gas density range.

$$CH_3 + HBr \rightarrow CH_4 + Br \qquad (1)$$

The pressures employed in the current study (up to 100 bar) are sufficient to completely quench any vibrationally excited species on the time scale of the experiments (>5 μs). If there was an interference of vibrationally excited species in the previous direct measurements and if the true rate constant is much lower (as the data obtained using VLPR infer), then a *decrease* in the rate constant with pressure is expected.

Another objective of this study was to search for a possible buffer gas density dependence of the rate constant of reaction 1. Such a dependence can be expected if the explanation of the negative activation energies based on the "chemically activated system" with the transition state below the energy level of the reactants[24] is correct. In this case, an *increase* of the rate constant with pressure is expected at elevated pressures. Currently, a reliable prediction neither of the scale of such a dependence nor of the transition pressure is possible due to the insufficient accuracy of the well depth and the "transition state" energy by ab initio calculations and the lack of data on relaxation of vibrationally excited weakly bound complexes.

Many reactions of combustion importance (such as dissociation/recombination reactions, reactions with chemical activation, etc.) are buffer gas density dependent. Elevated pressures are encountered in a number of systems of practical importance, such as rocket engine combustion chambers and internal combustion and diesel engines. In the past, the high-pressure limit rate constants as well as the whole pressure falloff dependence were often obtained via an extrapolation of the low and intermediate pressure data. The accuracy and reliability of this procedure depend on the range of densities used in the experimental measurements. High-pressure kinetic measurements were pioneered by Troe and Hippler[29,30] and were explored mainly in this group. There have been few kinetic studies at elevated pressures,[31−34] the majority employed static reaction cells with a single pulse illumination by photolytic light. Recently, Hippler et al. incorporated high-pressure flow system in the experimental approach.[35] A similar approach is used in the current work. This technique is still not sufficiently characterized. Characterization and evaluation of the performance of the experimental approach was the third objective of this work.

In the course of this study the rate constant of reaction of methyl radical with atomic bromine (reaction 2) was necessary for the reaction kinetic modeling.

$$CH_3 + Br \rightarrow CH_3Br \qquad (2)$$

This reaction was not studied previously. In this work, the rate constant of reaction 2 was determined relative to the rate constant of methyl radical self-reaction,

$$CH_3 + CH_3 \rightarrow C_2H_6 \qquad (3)$$

The results of these latter measurements are also presented.

Experimental Section

Experimental Setup. The experimental approach used in this study is based on the combination of a laser pulsed photolysis with transient UV−vis absorption spectroscopy. The sketch of the experimental setup is shown in Figure 1. The reactant mixture which contains free radical photolytic precursor ($(CH_3)_2CO$ or CH_3Br), reactant (HBr), and a buffer gas (He) in great excess (10^3-10^5 times) is slowly flowing through a high-pressure absorption cell. The cell (internal diameter 7.0 mm, internal length 10.4 cm, volume of 4.0 cm^3) is equipped with two 12.7 mm in diameter 12.7 mm thick fused silica windows and is designed to withstand pressures up to at least 150 bar. Typical reactant concentrations were $[(CH_3)_2CO] = (2.0-6.5)$

$\times 10^{15}$, [HBr] = (0.3−3.0) $\times 10^{16}$, and [CH_3Br] = (2.0−15) $\times 10^{16}$ molecules cm^{-3}. Much higher concentrations of acetone (up to 3.6 $\times 10^{16}$ molecules cm^{-3}) were used in several experiments aimed at the search of CH_3CO transient absorption. The energy flux of the laser light was varied in the range 1.2−21 mJ cm^{-2} ((1.2−20) $\times 10^{15}$ photon cm^{-2}). Attenuation of the laser light was performed by inserting flat non-UV grade quartz plates (with typical attenuation of ca. 50%-60% per plate) into the laser beam. Typical initial concentrations of methyl radicals were in the range (0.5−14) $\times 10^{14}$ molecules cm^{-3}. All experiments were performed at ambient temperature 297 ± 3 K and three buffer gas pressures − 1, 11, and 101 bar. A typical total flow rate of ca. 50 standard cubic centimeters per second was used. Experiments were performed under the conditions of complete replacement of the reaction mixture between laser pulses using proper repetition rates (e.g., 0.1 Hz at 100 bar).

Unfocused light from an ArF excimer laser (Lumonics TE−861T-3) formed into a beam by two iris diaphragms was reflected by a 45° (>98% at 193 nm, Newport) dielectric mirror and directed along the cell axis so that it fills all the cross section of the cell. When reflected by the dielectric mirror, the laser beam is merged with the monitoring beam which is formed by a fused silica lens (f = 10 cm). After passing the cell, the laser beam is separated from the monitoring light using the second 45° dielectric mirror for 193 nm.

Hollow cathode lamps (HCL) as well as low-power Xe and Hg arc lamps are used as sources of the monitoring light. Methyl radicals were monitored using strong narrow absorption band around 216 nm.[36−40] A 216.51 nm line from a copper hollow cathode lamp was used as a source of the monitoring light. To improve the monitoring light intensity, a three-electrode hollow cathode lamp (Superlamp, Photron) was used with current boosting. A high-voltage pulse generator (Cober 605P) provided 1.8 kV, 10 A flat-top pulses with durations up to 10 ms. Typically, rectangular pulses with a duration of 3 ms and current of 4 A were used. The estimated gain in light intensity (compared to a regular hollow cathode lamp operating at 10 mA) was ca. 2000 times. Concentration of HBr was monitored in situ using UV absorption at the 196.0 nm line of a Se hollow cathode lamp. Formation of molecular bromine was ruled out based on the measurements of light absorption at 422 nm (Ne line from a HCL lamp).

The light from a hollow cathode lamp is focused into the cell and then onto the entrance slit of a grating monochromator (Jarrell-Ash, model 82-518, 0.5 m) using two fused silica lenses with focal lengths of 10 cm. The residual light from the excimer laser pulse was removed using a spatial filter (1 mm wire perpendicular to the slit placed in the focal spot of the second lens) and by a liquid filter (4 $\times 10^{-3}$ M solution NaOH in water, 1 cm). The liquid filter provides depression of 193 nm light 10^{12} times while attenuating the monitoring light (216.5 nm) only by 17%. A photomultiplier tube (Hamamatsu R106) mounted on the exit slit operates on a reduced number of dynodes (6) with a voltage divider current of 2.7 mA, which ensures good linearity and lower noise at high photon fluxes. The PMT signal is preamplified (EMI preamplifier), then digitized and stored using a digital storage oscilloscope (LeCroy 9310A, Dual channel, 400 MHz, 100 Msamples/s, 50 Kpts/ch). The time resolution is determined by the preamplifier setting and can be 30 ns, 0.3 μs, 3 μs, or 30 μs. Typically, a 0.3 μs time constant was used. After the signal accumulation (typically, from 300 to 800 pulses), the traces were transferred to a PC for processing and fitting.

The second monochromator (Jarrell-Ash, model 82-518, 0.5 m) was used for in situ monitoring of HBr and Br_2. For this purpose, a proper hollow cathode lamp was installed in the working position. The first dielectric mirror was removed. The monitoring light is reflected by the second mirror, focused on the entrance slit of the second monochromator, and measured by a (Hamamatsu R106) photomultiplier. A standard circuit for current modulation and lock-in detection from an atomic absorption spectrometer was used in these measurements.

A light shutter (Oriel model 76993) was located between the laser and the cell. Every odd laser pulse was blocked. A synchronized switch (Pasternack Electronics, PE7100) was used to connect the two input channels of the oscilloscope to the preamplifier output to accumulate separately the light intensity profile with and without the laser pulse entering the reactor. This procedure was used to account for a small (0.5% in 1 ms) variation of the monitoring light intensity during a pulse. The two traces then were used to calculate the temporal profile of the monitoring light absorption.

The high-pressure flow system consists of high-pressure mass flow controllers, a high-pressure flow cell, an upstream (back) pressure regulator, high-pressure test gauges, and the cylinders with the helium, the precursor, and the reactant mixtures. Brooks high-pressure mass flow controllers (5850 TR series) are used. The flow controllers were periodically calibrated using the soap film method. In the initial experiments, a pneumatically controlled upstream pressure regulator (Grove MITY-MITE model 5D91W, up to 2000 psi) was used. Later, it was replaced by an electronic upstream pressure regulator (Brooks, model 5866). Both upstream pressure regulators demonstrated comparable performance, the electronic being more convenient. The flow reactor pressure was measured using test pressure gauges (Matheson model 63-5633M, up to 250 bar, model 63-5622 M, up to 14 bar, accuracy 0.25%) and by the internal calibrated pressure sensor of the electronic upstream pressure regulator.

Reactants and Preparation of Mixtures. Helium from Matheson (UHP grade, 99.999%) was passed through an oxygen trap (R&D Separations, OT3-2) to ensure molecular oxygen content less than 0.02 ppm. A mixture of acetone in helium (15.2 ± 0.5 ppm) was prepared in a 40 L high-pressure tank. Approximately 10 days were allowed for mixing before the first use of the mixture. The acetone concentration in the mixture was determined using gas chromatography.

Hydrogen bromide (Matheson, initial purity 99.8%) was purified by a multiple (6−7 times) liquid nitrogen cooled trap-to-trap distillation with passing through a trap cooled by melting ethanol (−115 °C, HBr vapor pressure ca. 20 Torr, Br_2 vapor pressure ca. 1 $\times 10^{-4}$ Torr), degassed, and stored in a 5 L darkened Pyrex glass flask. The content of molecular bromine (and other low volatile impurities) after the purification was estimated based on the pressure developed in smaller volume (400 cm^3) by vaporization of the residual material trapped in the melting ethanol trap. The content of impurities (including molecular bromine) was determined to be less than 0.007%.

Methyl bromide (Liquid Carbonic, 99.5%) was degassed from liquid nitrogen and purified by multiple trap-to-trap distillation.

Mixtures of HBr with He and CH_3Br with He at a pressure of 150 bar were prepared before each series of experiments in a stainless steel high-pressure vessel (Parr, high-pressure reactor, 300 mL, model 4561 M). Pressures of HBr and CH_3Br were measured using MKS Instruments pressure gauges for the ranges 0−10 Torr, 0−100 Torr, and 0−1000 Torr. The total final

pressure was measured by a pressure gauge installed on the high-pressure vessel. Several possible sources of errors were identified in the quantitative preparation of mixtures at high pressures. Efficient stirring must be provided due to the very slow diffusion at elevated pressures. The vessel was equipped by the manufacturer with an electrical motor driven vane stirrer. This approach was found to be unacceptable due to the high "dead volume" of the sealing glands of the stirrer. Instead of the original stirrer, a regular Teflon coated magnetic bar driven magnetically through the bottom wall (nonferromagnetic stainless steel) of the vessel was used. This provides fast and efficient mixing inside the high-pressure vessel. Second, loading of the vessel with helium at elevated pressures leads to a significant temperature rise. This elevated temperature dissipates quite slowly when no stirring is applied. However, cooling is efficient under stirring. The gas temperature was monitored using an internal thermocouple (supplied with the vessel). The gas mixture was cooled until the difference between the gas temperature and the ambient temperature was less than 3 K. A proper correction for the residual temperature difference was made in the mixture composition calculations.

The problem of a "dead volume" requires separate consideration. The "dead volume" is composed by the volume of the tubes leading to the connection valves, pressure gauge, etc. No stirring can reach inside the dead volume. Slow diffusion requires too long time to exchange the gas and equalize the composition. An estimate gives the characteristic diffusion time at a distance of 5 cm of ca. 1 h at 150 bar He. There is significant "amplification" of the dead volume effect due to the fact that the component which is present in the mixture at low concentration (HBr or CH_3Br) and is supplied to the vessel first is compressed almost pure in the dead volume during the first stages of the second component (He) addition. The following expression was derived (see Appendix 1) using a model based on the assumption of perfect mixing in the bulk of the vessel during the mixture preparation:

$$x_1/x = x^{\alpha} \qquad \text{(E1)}$$

where x_1 is the actual mole fraction of the minor component in the bulk of the vessel, x is the targeted (overall) mole fraction, and $\alpha = V_{dead}/(V_{total} - V_{dead})$ is the ratio of the dead volume and the residual (total minus dead) volume of the vessel. For example, for a vessel with $\alpha = 0.05$ and targeted mole fraction of 0.01% ($x = 1 \times 10^{-4}$), the actual mole fraction in the bulk of the reactor would be $x_1 = 0.0001^{0.05}x = 0.63x$, which is in error by 37%. The larger is the fraction of the dead volume and the mixture dilution, the bigger is the error. To minimize possible errors due to the "dead volume" effect, the external outlets of the vessel were minimized and the gland used for the original stirrer axis sealing was removed. A conservative estimate on the dead volume is <5.4 cm^3, with the reactor volume of 300 cm^3. Therefore, the maximum possible error due to the "dead volume" effect for 0.1−0.2% mixtures (used in this study) is estimated to be less than 12%.

In the mixture preparation at elevated pressures as well as in the calculations of the concentrations in the flow reactor, proper corrections for nonideal gas behavior were made. The compression factor for He is Z_{He}(100 bar, 300 K) = 1.0471 and Z_{He}-(150 bar, 300 K) = 1.0735.[41]

Stability of HBr and in situ HBr Concentration Measurements. Special attention was paid to the stability of HBr during storage in the glass flask, in mixtures in the stainless steel vessel, and when passing through the stainless steel flow system. One portion of HBr was stored in a Pyrex glass flask over the more than one year period with no indication of HBr decomposition. Neither molecular hydrogen (as monitored via the residual pressure after freezing with liquid nitrogen) nor molecular bromine (as measured using visible absorption at 422 nm, see later) were found. Before being used, both the high-pressure vessel and the flow system were passivated with ca. 10 Torr of HBr. Mixtures of HBr with He prepared in the same day were used in the experiments. Several times the mixtures were left for the periods of 2−3 days, with subsequent check for the presence of Br_2. No Br_2 was detected in such experiments. Additional experiments were performed to determine whether there is a detectable decomposition of HBr when flowing through the mass-flow controllers, connecting tubes, and the flow reactor. Such measurements were performed both with the working mixtures and when only the mixture of HBr/He (0.1−0.2%) was allowed to the reactor. The 422 nm line (near the maximum of Br_2 absorption, absorption cross section ca. 5×10^{-19} cm^2 molecule^{-1} [42]) from Hg/Ne HCL was used. The gas flow was repeatedly replaced with flow of pure He, and the difference in the light intensity transmitted through the cell was measured. No change in the light intensity was observed within the experimental accuracy, which yielded an upper limit on molecular bromine present in the mixture $<2 \times 10^{15}$ molecules cm^{-3}. To increase the sensitivity of these measurements, the reactor was filled with HBr/He mixture (typically 1.4%) at a pressure of 20 bar. Then, the flow was stopped and the system was left with standing gas for 10 min. A flush flow of He was then let to the reactor and the light intensity at 422 nm was monitored. These experiments lead to an upper estimate of the possible Br_2 production less than 3×10^{-4} of the concentration of HBr in 10 min.

In a number of experiments, the concentration of HBr was measured in situ using UV absorption at 196.0 nm (Se HCL). The absorption cross section of hydrogen bromide at this wavelength is σ(HBr, 196 nm, 298 K) = 1.55×10^{-18} cm^2 molecule^{-1}.[43] The concentrations of HBr determined in this way agreed within ±3% (the accuracy of these measurements) with those calculated from the flow conditions—temperature, pressure, flow rates, and mixture compositions.

Generation of Methyl Radicals. Methyl radicals are produced using excimer laser photolysis (ArF, 193.3 nm) of acetone and methyl bromide:

$$(CH_3)_2CO + h\nu\ (193\ nm) \rightarrow 2CH_3 + CO \qquad \text{(4a)}$$

$$\rightarrow CH_3 + CH_3CO \qquad \text{(4b)}$$

$$CH_3Br + h\nu\ (193\ nm) \rightarrow CH_3 + Br(^2P_{3/2}) \qquad \text{(5a)}$$

$$\rightarrow CH_3 + Br^*(^2P_{1/2}) \qquad \text{(5b)}$$

Photolysis of acetone at 193 nm at pressures less than 1 bar was studied in detail previously.[44] Channel 4a was found to account for >99% of the overall photodissociation at low pressures. However, at elevated pressures, due to the much faster quenching of highly vibrationally excited acetyl radical, this was not guaranteed, and the importance of channel 4b at elevated pressures was investigated. The measurements in this work put 5% as an upper limit on the importance of the channel 4b at 100 bar He (see the Results section).

Role of Spin−Orbit Excited Br*($^2P_{1/2}$) Atoms. Electronically excited bromine atoms can be produced both in the photolysis of methyl bromide (5) and in the photolysis of hydrogen bromide (6):

$$HBr + h\nu\ (193\ nm) \rightarrow H + Br(^2P_{3/2}) \quad (6a)$$

$$\rightarrow H + Br^*(^2P_{1/2}) \quad (6b)$$

Donovan and Hussein[45] did not see excited bromine atoms in VUV photolysis of CH_3Br, $\phi_5(Br^*) = 0$. The quantum yield of Br* in photolysis of HBr is known ($\phi_6(Br^*) = 0.15$,[46] 0.14.[47] According to the most recent measurements, the rate constant of the collision quenching of spin−orbitally excited bromine atoms on He is $k_{Q,He}(Br^*) = 1.6 \times 10^{-14}$ cm^3 molecule^{-1} s^{-1}.[48] Such a collision quenching rate leads to the lifetime of excited Br atoms of 26 ns at 100 bar, 260 ns at 10 bar, and 2.6 μs at 1 bar. Therefore, excited bromine atoms play no role in our measurements (the shortest time used in the processing of the kinetic curves was 5 μs).

Absorption Cross Sections. Absorption cross sections of acetone, CH_3Br, and HBr at the laser wavelength 193.3 nm as well as at the monitoring wavelength 216.51 nm are required in the numerical fits of the absorption temporal profiles. Some of these data were taken from literature; others were measured in this work. The measurements of acetone cross section at 193.3 nm were performed using the high-pressure flow cell by monitoring the laser pulse intensity by a combination of a fluorescent quartz and a photodiode. These measurements were performed under single-pulse conditions. Laser intensity transmitted through the cell was compared to that when the acetone/helium mixture was replaced with pure helium. Absorption of 193 nm light by acetone is found to be buffer gas pressure dependent. This is due to the pressure broadening of the resolved vibrational structure in the absorption spectrum of acetone near 193 nm. The absorption cross section of methyl radical at 216.51 nm was also found to be pressure dependent.[31,49] For the species which exhibit broad structureless absorption bands (such as HBr) the independence of the absorption cross sections of pressure was assumed.

The Beer−Lambert plots for acetone absorption at 193 nm at different pressures are shown in Figure 2. The absorption cross section data are summarized in Table. 1. Absorption cross sections of methyl radicals were calculated from the initial signal amplitudes in the photolysis of acetone alone, the decay parameters, and the rate constant data on the methyl radical recombination reaction 3. Fitting the temporal profiles of absorption in this case allows the ratio of the recombination rate constant and the absorption cross section of methyl radicals at the wavelength of the monitoring light, $k_3/\sigma_{216.51}(CH_3)$, to be obtained. The literature data[40] were used to extract the cross section of methyl radicals from the experimentally measured ratios. While fluxes of laser radiation were measured several times, they were not used in any quantitative data processing. These flux measurements agree with indirect photon flux estimates obtained from the methyl radical absorption cross sections, cross sections of absorption of laser light by acetone, and acetone concentrations in the absorption cell.

Data Processing. Experimental temporal light intensity profiles were fitted by numerical solutions of a system of ordinary differential equations, which corresponds to the chosen set of elementary reactions. The SCIENTIST software (MicroMath) was used to perform nonlinear least-squares fits of the experimental light intensity profiles by a numerical solution of a dimensionless system of differential equations using approach outlined in Appendix 2.

Reaction Mechanism. The initial free radical concentrations used in the current work are relatively high, and radical−radical reactions are of substantial importance. The reaction mechanism

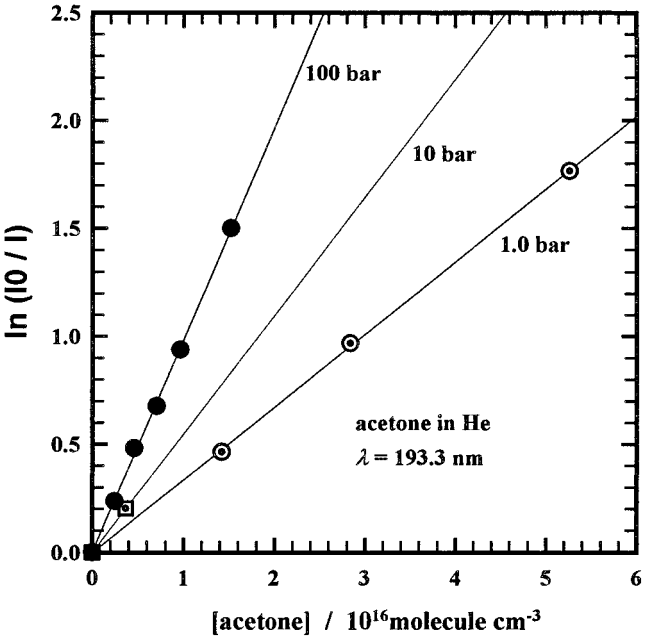

Figure 2. Beer−Lambert plot for the ArF laser light (193.3 nm) absorption by acetone at different buffer gas (He) pressures.

used to fit the experimental profile consists of the reaction under study (reaction 1), reaction of methyl radicals with bromine atoms (reaction 2), reaction of recombination of methyl radical (reaction 3), and several additional undesirable secondary reaction 7−11:

$$CH_3 + H \rightarrow CH_4 \quad (7)$$

$$H + HBr \rightarrow H_2 + Br \quad (8)$$

$$H + H \rightarrow H_2 \quad (9)$$

$$H + Br \rightarrow HBr \quad (10)$$

$$Br + Br \rightarrow Br_2 \quad (11)$$

In the reaction mechanism, all radical−molecule reactions, except for the reaction under study (reaction 1) and reaction 8, are neglected. Reactions of all free radicals (CH_3, H, Br) with $(CH_3)_2CO$, CH_4, CH_3Br, CO, and H_2 are too slow at ambient temperature to play any role. Reactions of CH_3 and H with Br_2 are fast. However, only minor concentrations of molecule bromine are formed during the reaction. Model calculations have shown that taking into account reactions of CH_3 and H with molecular bromine has less than 0.6% effect on the extracted rate constant of reaction 1. Therefore, reactions of free radicals with molecular bromine were also neglected.

The most important interfering reaction is reaction 2, reaction of methyl radicals with bromine atoms (which are formed initially in the photolysis of HBr, and later after the pulse in the reaction of methyl radicals with HBr (reaction 1)) and reaction of hydrogen atoms (formed in the photolysis of HBr) with HBr (reaction 8)). Reaction 2 was characterized in this study using photolysis of CH_3Br as a photolytic source of CH_3 radicals and Br atoms with equal initial concentrations. The absorption cross section of methyl radical at the monitoring wavelength was determined via the measurements of the transient absorption profiles in the photolysis of acetone alone, when reaction 3 is the only reaction responsible for the consumption of methyl radicals. The literature data[40] on the recombination reaction 3 were used in this work.

TABLE 1: Absorption Cross Sections of Some Molecules at 193.3 nm (ArF Laser) and at 216.51 nm (Cu Hollow Cathode Lamp) (298 ± 2 K and 1−100 Bar)

species	absorption cross section at 193.3 nm, cm^2 $molecule^{-1}$	comment	absorption cross section at 216.51 nm, cm^2 $molecule^{-1}$	comment
$(CH_3)_2CO$	$(9.45 \pm 0.05) \times 10^{-18}$	$p_{He} = 100$ bar	$(1.49 \pm 0.10) \times 10^{-19}$	$p_{He} = 100$ bar
	$(5.27 \pm 0.40) \times 10^{-18}$	$p_{He} = 10$ bar		$p_{He} = 10$ bar
	$(3.23 \pm 0.07) \times 10^{-18}$	$p_{He} = 1$ bar	$(1.8 \pm 0.1) \times 10^{-21}$	$p = 1$ bar, air
		this work	$(1.47 \pm 0.10) \times 10^{-21}$	120 Torr acetone, this work
HBr	$(1.78 \pm 0.01) \times 10^{-18}$	ref 50	$(3.44 \pm 0.10) \times 10^{-19}$	ref 50, confirmed in this work
CH_3Br	$(4.49 \pm 0.07) \times 10^{-19}$	ref 51	$(3.48 \pm 0.05) \times 10^{-19}$	ref 51
CH_3			1.71×10^{-17} at 100 bar He; 3.20×10^{-17} at 10 bar, He; 3.52×10^{-17} at 1.0 bar He	using the experimentally determined ratios $k_3/\sigma_{216.51}(CH_3)$ (Table 3) and the literature data on k_3 (Table 2)

TABLE 2: Rate Constants for the Reactions Used in the Kinetic Modeling

reaction	rate constant (cm^3 $molecule^{-1}$ s^{-1})	reference/comment
$CH_3 + CH_3 \rightarrow C_2H_6$	6.47×10^{-11} at 100 bar He	k_{inf} from ref 40,
	6.42×10^{-11} at 10 bar He	pressure falloff
	6.29×10^{-11} at 1 bar He	from ref 52
$CH_3 + H \rightarrow CH_4$	4.62×10^{-10} at 100 bar He	k_{inf} from ref 53,
	4.37×10^{-10} at 10 bar He	pressure falloff
	3.27×10^{-10} at 1 bar He	from ref 54
$H + HBr \rightarrow H_2 + Br$	6.32×10^{-12}	ref 55
$H + Br \rightarrow HBr$	2.25×10^{-11} at 100 bar He	calculated as $k_{H+Br} = 2(k_{Br+Br}k_{H+H})^{1/2}$
	2.25×10^{-12} at 10 bar He	
	2.25×10^{-13} at 1 bar He	
$Br + Br \rightarrow Br_2$	7.64×10^{-12} at 100 bar He	ref 56
	7.64×10^{-13} at 10 bar He	
	7.64×10^{-14} at 1 bar He	
$H + H \rightarrow H_2$	1.66×10^{-11} at 100 bar He	ref 57
	1.66×10^{-12} at 10 bar He	
	1.66×10^{-13} at 1 bar He	
$CH_3 + Br \rightarrow CH_3Br$	$k_2/k_3 = 1.65 \pm 0.26$ at 100 bar He,	this work, 95%
	1.15 ± 0.30 at 10 bar He,	confidence interval
	0.92 ± 0.32 at 1 bar He	
$CH_3 + HBr \rightarrow CH_4 + Br$	to be determined	

Reactions 2, 3, 7, and 9−11 are buffer gas density dependent. Recombination of methyl radicals is close to the high-pressure limit, reactions of methyl radicals with Br and H atoms are in the pressure falloff region, and reactions of atom recombination 9−11 are in the low-pressure limit over the experimental pressure range 1−100 bar. Reactions 9−11 play a minor role even at 100 bar and a negligible role at 1 bar. The rate constant of the reactions used in the kinetic modeling are listed in Table 2.

Results

Methyl Radical Absorption at 216.51 nm. Absorption temporal profiles recorded at 1, 11, and 100 bar (He) in the photolysis of acetone alone were used to obtain the ratio of the rate constant of recombination reaction 3 and the methyl radical absorption cross section. An example of the absorption profile is shown in Figure 3. The results are given in Table 3.

Acetyl Radical Production in Photolysis of Acetone at 193 nm. Photolysis of acetone was shown to be a very clean source of methyl radicals at pressures below 1 bar.[44] However, this does not warrant the performance of this precursor at elevated pressures. At higher pressures, the collisional relaxation of vibrationally excited acetyl radicals produced in the primary photolytic process is faster and thus it is not clear whether it can lead to significant stabilization of acetyl radicals or not. Absorption profiles were recorded at 222.57 and 224.42 nm where acetyl radical has strong absorption ($\sigma_{224}(CH_3CO) \approx 1 \times 10^{-17}$ cm^2 $molecule^{-1}$ [58]). The results are illustrated in Figure 4. An upper limit of 5% ($f_{4b} < 0.05$ at 100 bar He) for the route 4b was derived from these measurements. An estimate based on the RRKM theory is in accord with this conclusion. The collisional quenching at 100 bar He is expected to provide less than 5% stabilization yield of CH_3CO radicals when the excess energy of the radicals (energy above the dissociation threshold, E^+) is larger than 60 kJ mol^{-1}. The maximum

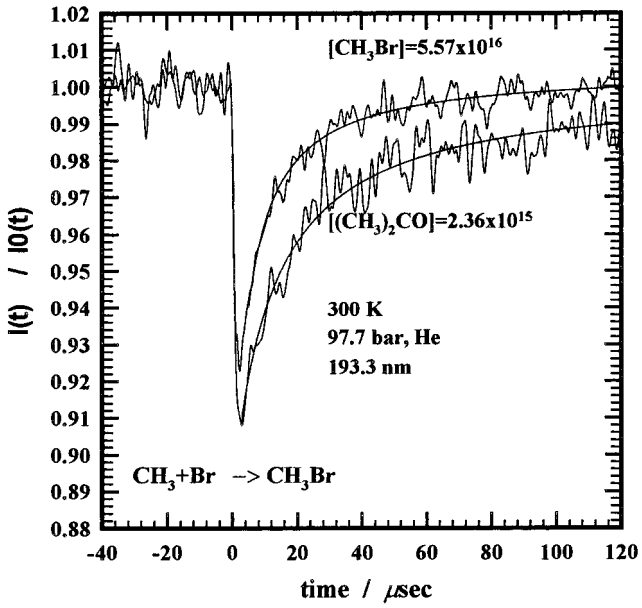

Figure 3. Transient absorption of methyl radicals (recorded at 216.51 nm) in photolysis of acetone and methyl bromide at 193.3 nm. The solid curves are the results of the fits.

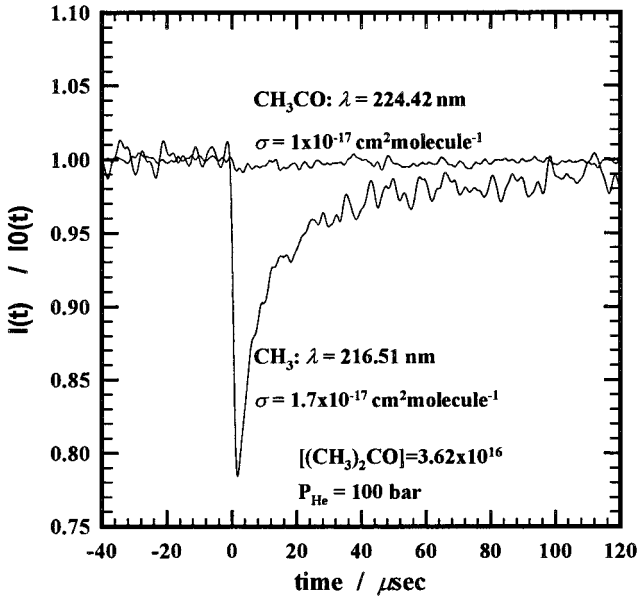

Figure 4. Transient absorptions recorded in photolysis of large concentration of acetone at 216.51 nm (CH_3 radical) and 224.42 nm (CH_3CO radical).

TABLE 3: The Ratio $B = k_3/\sigma_{216.51}(CH_3)L$ for Recombination of CH_3 Radicals ($T = 301 \pm 1$ K, Buffer Gas is He, and Cell Length, L, = 10.4 cm

He pressure/bar	$(k_3/(\sigma_{216.51}(CH_3)L))/10^6\ s^{-1}$
1.05	0.172 ± 0.007
11.2	0.193 ± 0.008
101	0.365 ± 0.016

TABLE 4: Rate Constant for the Reaction $CH_3 + Br$ ($T = 301 \pm 1$ K)

He pressure (bar)	$k_{CH_3+Br}/k_{CH_3+CH_3}$ [a]	$k_{CH_3+CH_3}$ [b]	k_{CH_3+Br} [a,c]
1.05	0.92 ± 0.32	6.29×10^{-11}	$(5.8 \pm 2.2) \times 10^{-11}$
11.2	1.15 ± 0.30	6.42×10^{-11}	$(7.4 \pm 2.2) \times 10^{-11}$
101	1.65 ± 0.26	6.47×10^{-11}	$(10.7 \pm 2.3) \times 10^{-11}$
∞			$(11.9 \pm 2.5) \times 10^{-11}$ [d]

[a] This work, the errors indicate 95% confidence interval. [b] Based on $k_{inf} = 6.5 \times 10^{-11}$ cm^3 molecule^{-1} s^{-1} (ref 40) and the pressure falloff parameters from ref 52. [c] The errors were obtained by combining the errors in the rate constant ratios (95% confidence interval, column 2) with the error in the rate constants $k_{CH_3+CH_3}$. The latter was estimated as 14% by addition of the error stated in the original publication (ref 40) and the deviation from the value suggested in the review paper (ref 57) (ca. 8%). [d] High pressure limit rate constant obtained by a short extrapolation (this work).

theoretically possible excess energy of acetyl radicals produced in the photolysis of acetone at 193 nm is 266 kJ mol^{-1}.

Reaction $CH_3 + Br \rightarrow CH_3Br$. Photolysis of methyl bromide (5) was used as a simultaneous photolytic source of methyl radicals and bromine atoms. The photolytic route (5) is expected to be the main channel of photodissociation of CH_3Br in the ultraviolet region.[42,59] Therefore, the equality of the initial concentrations of methyl radicals and bromine atoms is provided. Figure 3 shows the experimental profiles recorded in photolysis of acetone and methyl bromide with equal initial concentrations of methyl radicals. The role of reaction 2 is apparent. Such measurements allow determination of the ratio of the rate constant of reaction of methyl radicals with Br atoms and the methyl radical recombination reaction, k_2/k_3. The results are listed in Table 4.

Reaction $CH_3 + HBr \rightarrow CH_4 + Br$. The experimental conditions and the results of the experiments to measure rate

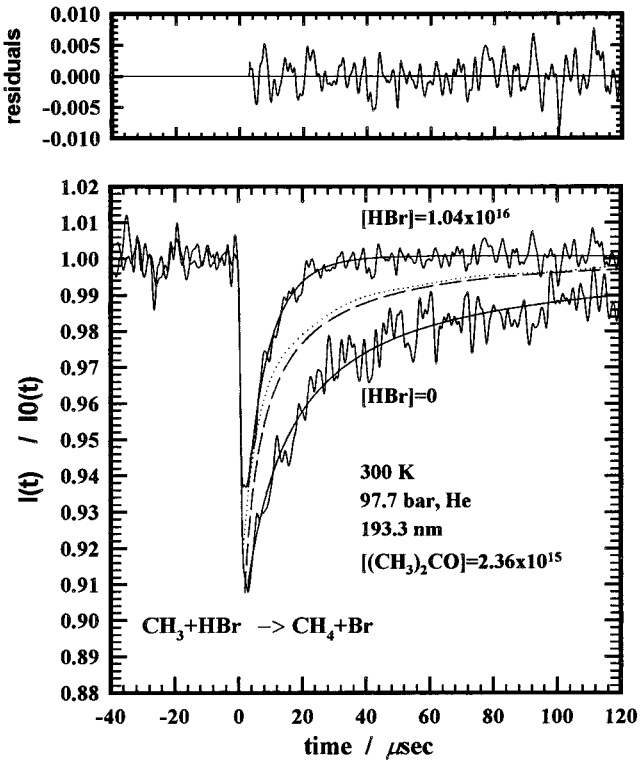

Figure 5. Transient absorption of methyl radicals without and with HBr added. The solid lines through the experimental points show the fitted line using the reaction model (see text for details). The plot on the top shows the residuals of the fit. The dashed line is a simulated kinetic curve in the presence of the same concentration of HBr and without reaction 1 ($k_1 = 0$) but with other secondary reactions taken into account. The dotted line is calculated with the rate constants of reactions 2, 3, and 7 set to their uncertainty limits; rate constant k_3 is increased by 14%, the ratio k_2/k_3 is increased by 16%, and the rate constant k_7 is increased by a factor of 2.5.

constant of reaction 1 are summarized in Table. 5. An example of the absorption profiles of methyl radicals at 216.51 nm at 100 bar He with and without HBr added is shown in Figure 5. Side reactions of methyl radical with itself, Br, and H atoms play a significant role and can account for from 40−80% (at 100 bar) of the rate of consumption of methyl radical depending on the laser pulse energy (in the time domain used for the data processing). The dashed curve in Figure 5 shows the kinetic curve simulated with all reactions in the mechanism taken into account but reaction 1. The difference between the dashed curve and the experimental profile is due to reaction 1. The dotted curve was simulated in a similar manner to the dashed curve, but with the rate constants of reactions 2, 3, and 7 set at their uncertainty limits (see the figure caption). The relative importance of the secondary interfering reactions increases with pressure. Contribution of these reactions is relatively small at 1 bar and significant at 100 bar. This is mainly due to the increase with pressure of the rate constants of the main interfering reactions 2 and 7.

To verify the experimental and the data processing procedures, the following checks were performed. At fixed concentration of HBr, the laser light intensity was varied by a factor of 4 at 1 bar, factor of 7 at 11 bar, and factor of 16 at 100 bar. Investigation of Table 5 shows no systematic dependence of the pseudo-first-order rate constant returned by the fits on the laser pulse energy. Concentration of HBr was varied within the factor 5−6. The pseudo-first-order rate constants of reaction 1 returned by the fits were plotted as a function of HBr concentration. The results for 1, 11, and 100 bar buffer gas

TABLE 5: Experimental Conditions and Results to Measure Rate Constant of CH_3 + HBr → CH_4 + HBr Reaction

[acetone] 10^{15} molecule cm^{-3}	[HBr] 10^{15} molecule cm^{-3}	$[CH_3]_0$[a] 10^{14} molecule cm^{-3}	$[Br]_0 = [H]_0$[b] 10^{14} molecule cm^{-3}	laser energy flux mJ cm^{-2}	k_1' 10^3 s^{-1} [c,d]
		$P_{He} = 1.05$ bar			
6.11	13.6	2.5	1.6	6.1	42.2 ± 2.9
6.03	23.2	2.0	2.1	4.8	62.4 ± 4.9
6.47	9.41	2.0	0.82	4.6	26.6 ± 2.8
5.07	8.98	0.92	0.45	2.7	38.1 ± 1.6
5.07	8.98	3.8	1.8	11	30.7 ± 2.2
5.07	8.98	1.5	0.73	4.3	20.1 ± 1.4
5.14	4.44	1.2	0.29	3.5	16.7 ± 1.4
		$P_{He} = 11.2$ bar			
3.99	35.1	2.4	3.5	5.8	130 ± 14
4.03	13.8	3.0	1.7	7.3	51.8 ± 4.6
4.08	4.54	2.8	0.52	6.6	25.3 ± 2.3
3.98	24.3	3.1	3.2	7.6	91.7 ± 7.0
3.59	7.96	7.0	2.6	19	29.8 ± 2.9
3.59	7.96	0.96	0.36	2.6	29.8 ± 6.7
3.59	7.96	3.2	1.2	8.7	30.3 ± 3.3
		$P_{He} = 101$ bar			
3.48	13.9	12	4.3	18	52.4 ± 9.1
3.48	26.0	7.1	5.0	11	80 ± 19
2.99	22.1	4.2	2.9	7.6	101 ± 16
2.99	18.7	2.9	1.7	5.3	60 ± 10
2.7e	16.7	2.6	1.5	5.1	51 ± 10
2.46	9.46	2.4	0.85	5.2	28.4 ± 4.8
2.46	9.46	6.5	2.4	14	30.4 ± 4.3
2.46	9.46	0.86	0.31	1.9	21 ± 10
2.46	4.73	3.1	0.55	6.8	21.3 ± 4.1
2.46	4.73	7.3	1.3	16	24.5 ± 3.3
2.44	9.79	0.94	0.35	2.1	25.2 ± 8.5
2.44	4.89	1.0	0.19	2.3	9.7 ± 9.8
2.44	20.4	0.92	0.72	2.0	62 ± 11
2.44	6.13	0.57	0.13	1.3	33.2 ± 7.4
2.44	12.3	0.86	0.41	1.9	32.7 ± 7.0
2.47	20.5	1.6	1.29	3.6	57.7 ± 7.4
2.47	6.17	1.3	0.30	2.9	23.1 ± 4.1
2.47	12.3	1.0	0.49	2.3	52 ± 11
2.36	10.4	8.6	3.5	20	52.6 ± 4.4
2.36	10.4	1.4	0.60	3.3	54.4 ± 8.1

[a] Initial concentration of methyl radicals. [b] Initial concentrations of bromine and hydrogen atoms. [c] Pseudo-first-order rate constant of reaction 1, $k_1' = k_1$[HBr]. [d] The errors indicated are ±3 standard deviations of the fits and reflect statistical accuracy only.

pressure are shown in Figure 6. Linear dependencies are observed, as expected. The scatter of the experimental points increases at high pressures. This is due to both the decreasing quality of the kinetic curves at 100 bar and to the increasing role of the interfering reactions. The quality of the kinetic curves deteriorates due to two main reasons: the decrease of the absorption coefficient of methyl radical due to the pressure broadening and the lesser number of averaging due to the much lower pulse repetition rate.

The slopes of the linear regression lines in Figure 6 were used to determine the rate constant of reaction 1 at different pressures. The results obtained in this way are $k_1 = (2.9 \pm 0.7) \times 10^{-12}$, $(3.8 \pm 1.5) \times 10^{-12}$, and $(3.4 \pm 1.3) \times 10^{-12}$ cm^3 molecule^{-1} s^{-1} at the buffer gas (He) pressures of 1.05, 11.2, and 101 bar, respectively.

Error Assessment. The error assessment in the case when a number of interfering reactions are to be taken into account represents a rather complex problem. To assess the error in the determined rate constants, the following approach was used. First, for given experimental conditions (temperature and pressure), one experimental kinetic curve out of those that have maximum impact on the value of the determined rate constant (such as those at highest concentration of HBr in Figure 6) was chosen. Then, the sensitivities (S_j, eq E2) of the rate constant of reaction 1, k_1, obtained in fits by the reaction mechanism 1−3 and 7−11, to the different input parameters P_j, were determined by varying the input parameters by 10%,

$$S_j = \partial \ln(k_1')/\partial \ln(P_i) \qquad \text{(E2)}$$

The total error in k_1 was estimated assuming that the individual errors in the input reaction rate constants, absorption cross sections, and the uncertainties of the experimental parameters (acetone and HBr concentrations) are statistically independent,

$$\delta \ln(k_1) = (\Sigma_j |S_j\, \delta \ln(P_j)|^2 + |\delta \ln(k_1)_{st}|^2)^{1/2} \qquad \text{(E3)}$$

where $\delta \ln(k_1)$ is the total (logarithmic) error in k_1, $\delta \ln(P_j)$ are the logarithmic errors in the parameters used (rate constants of reactions 2, 3, and 7−11, absorption cross-sections, and the reactant concentrations), and $\delta \ln(k_1)_{st}$ is the statistical error in the determination of the rate constants due to the scatter of the experimental data. Three standard deviations of the linear regressions in Figure 6 were used as the measure of the statistical accuracy. The sensitivities determined in this way, the errors in the rate constants and other parameters used, and the total errors determined are summarized in Table 6.

Discussion

The rate constant of reaction 1 as a function of the buffer gas density, together with the results of previous measurements,

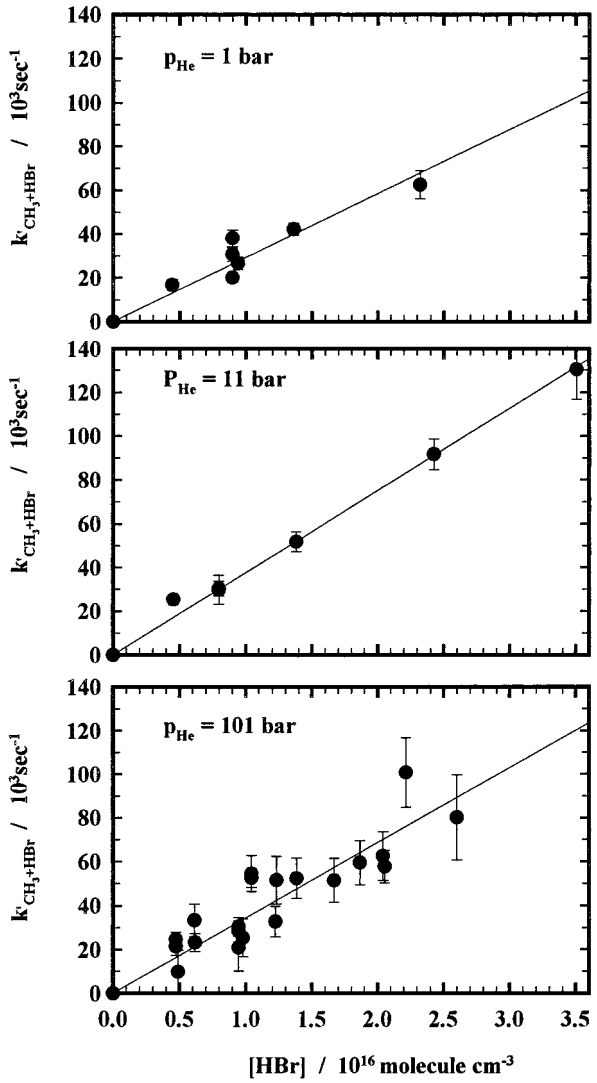

Figure 6. Pseudo-first-order rate constant of reaction 1 yielded by the fits of the experimental profiles plotted vs concentration of HBr at different buffer gas pressures.

is plotted in Figure 7. The current measurements together with the previous measurements cover the density range of 4.6 decades. The results indicate no dependence of the rate constant of reaction 1 on the buffer gas density. While the points at 11 and 100 bar are 14−25% higher than the low-pressure values, this deviation is within the experimental error.

Correction for Diffusion Control. At the highest density (at pressure 100 bar) a correction for the reactant diffusion control might be nesessary.[60] The rate constant of a bimolecular reaction is given by the Smoluchowski theory:

$$1/k = 1/k_{diff} + 1/k_{kin} \quad \text{(E4)}$$

$$k_{diff} = 4\pi R_{AB} D_{AB} \quad \text{(E5)}$$

where k_{diff} and k_{kin} are the diffusion-controlled and the kinetically controlled rate constants, respectively, R_{AB} is the "reaction radius" (the separation between the centers of the reactants molecules at the diffusion "bottleneck"), $D_{AB} = D_A + D_B$ and is the relative diffusion coefficient of the reactants, and D_A and D_B are the diffusion coefficients of the reactants.

The estimated relative diffusion coefficient $D_{(CH3-HBr)\text{ in He}}$ (300 K, 100 bar) = 1.35×10^{-2} cm^2 s^{-1} (based on $D_{HBr\text{ in He}}$ (300 K, 1 bar) = 0.657 cm^2 s^{-1}, $D_{CH3\text{ in He}}$ (300 K, 1 bar) = 0.691 cm^2 s^{-1}, calculated using the following Lennard-Jones parameters:[61] σ_{He}= 0.255 nm, ϵ_{He} = 10.22 K, σ_{HBr} = 0.335 nm, ϵ_{HBr} = 449 K, σ_{CH3} = 0.382 nm, ϵ_{CH3} = 148 K). Estimation the reaction radius as the separation between the H atom and C atom in the transition state, R_{AB} = 0.162 nm[20] leads to the diffusion-controlled rate constant (E5) $k_{diff} = 2.51 \times 10^{-11}$ cm^3 molecule^{-1} s^{-1} at 100 bar He. Using eq E4, this gives ca. +15% correction to the experimentally measured rate constant, $k_{kin} = 3.96 \times 10^{-12}$ cm^3 molecule^{-1} s^{-1} at 100 bar pressure. The correction at 10 bar is ca. 1.5% and can be neglected. The open symbol in Figure 7 shows the value corrected for the diffusion at 100 bar.

It should be mentioned that the expressions E4 and E5 are applicable for spherical reactants when the mean free path is smaller than the reactant separation at the closest contact. Neither of these two assumptions is fulfilled in our case. Both the mean free path of the reactants and the mean separation between the buffer gas atoms are larger than the reaction radius so that the assumption of continuous diffusion is hardly applicable. The reaction is nonisotropic, which should lead to a reduction of k_{diff} and, subsequently, to an increase in the corrected rate constant of reaction 1.

Role of the Excess Vibrational Energy. The maximum theoretically possible internal energy of methyl radicals formed in photodissociation of acetone at 193.3 nm (reaction 4a) is 219 kJ mol^{-1}. The characteristic relaxation time of a highly excited molecule, τ, can be estimated as

$$\tau = E/(\nu\langle\Delta E\rangle) \quad \text{(E6)}$$

where E is the internal energy, ΔE is the mean energy transferred in collision, and ν is the collision frequency. At 100 bar He, the collision frequency is ca. 1.2×10^{12} collisions/s. The mean energy transferred in collision of a highly vibrationally excited molecule with helium atom is 2−11 kJ mol^{-1}.[62] This leads to $\tau = (1.7-9.1) \times 10^{-11}$ s and $(1.7-9.1) \times 10^{-9}$ s at 100 and 1 bar He, respectively. At the lowest pressure of the current experiments, 1 bar, assuming the most conservative estimate (9×10^{-9} s), this time is still ca. 500 times shorter than the minimum time after photolysis used to process the experimental data (5 μs). At low excitation levels (such as single vibrational quantum), the above estimate is not applicable. The slowest vibrational relaxation experimentally observed for multiatomic molecules is that of methane.[63−65] Relaxation of methane in collisions with methane molecules and He atoms requires ca. 2×10^4 collisions.[63,64] The Lambert−Salter correlation[65] of the efficiency of vibrational relaxation with the frequency of the lowest vibrational mode infers 2 orders of magnitude higher rate for the vibrational relaxation of methyl radical compared to methane due to the much lower frequency of the out-of-plane vibration (ca. 606 cm^{-1}) compared to the lowest vibrational mode in methane (1306 cm^{-1}). The relaxation of the out-of-plane vibration (umbrella) mode of methyl radical in collisions with CH_3I is very fast and requires only ca. 40 collisions.[66] However, even under the assumption that the rate of vibrational relaxation of methyl radical is as slow as the rate of relaxation of methane, the estimated relaxation time (1.6 μs at 1 bar and 16 ns at 100 bar) ensures complete V−T relaxation in our experiments. Therefore, irrespective of which mode of relaxation (relaxation of the highly or low vibrationally excited molecules) is considered, the estimates unambiguously show complete thermalization of the excess energy under our experimental conditions. The agreement of our measurements with the measurements which employed lower buffer gas densities

TABLE 6: Sensitivities of the Determination of the Rate Constant of the Reaction CH_3 + HBr → CH_4 + Br from the Reaction Modeling and the Errors Assessment

parameter, P_i	sensitivity, $\partial\ln(k_1')/\partial\ln(P_i)$ at 1 bar	parameter relative error, $\delta(\ln(P_i))$	sensitivity, $\partial\ln(k_1')/\partial\ln(P_i)$ at 11 bar	parameter relative error, $\delta(\ln(P_i))$	sensitivity, $\partial\ln(k_1')/\partial\ln(P_i)$ at 100 bar	parameter relative error, $\delta(\ln(P_i))$
k_3	0.38	0.060	0.73	0.057	0.63	0.057
k_2/k_3	−0.28	0.35	−0.29	0.26	−0.14	0.16
k_7	−0.21	0.90[a]	−0.39	0.90	−0.37	0.90
k_8	0.13	0.15	0.16	0.15	0.17	0.15
k_9	1.5×10^{-4}	1.1[b]	1.1×10^{-3}	1.1	0.018	1.1
k_{10}	6.6×10^{-4}	1.2	0.0030	1.27	0.046	1.2
k_{11}	3.3×10^{-4}	0.25	8.2×10^{-4}	0.25	0.027	0.25
B	−0.84	0.040	−1.1	0.041	−1.7	0.044
[acetone]	0.67	0.030	1.0	0.030	1.4	0.030
[HBr]	−1.5	0.030	−1.7	0.030	−2.3	0.030
σ_{193}(acetone)	0.67	0.020	1.0	0.076	1.4	0.020
σ_{193}(HBr)	−0.76	0.0050	−1.0	0.0050	−1.6	0.0050
σ_{193}(CH_3Br)	0	0.015	0	0.015	0	0.015
σ_{216}(acetone)	-3.3×10^{-4}	0.070	-1.6×10^{-3}	0.74	0.068	0.070
σ_{216}(HBr)	−0.26	0.030	−0.39	0.030	−0.40	0.030
σ_{216}(CH_3Br)	0.018	0.014	0.019	0.014	0.065	0.014
statistical error (3 st. dev.)		0.048		0.013		0.044
cumulative relative error		0.26		0.40		0.39

[a] Corresponds to an uncertainty factor 2.5. [b] Corresponds to an uncertainty factor 3.0.

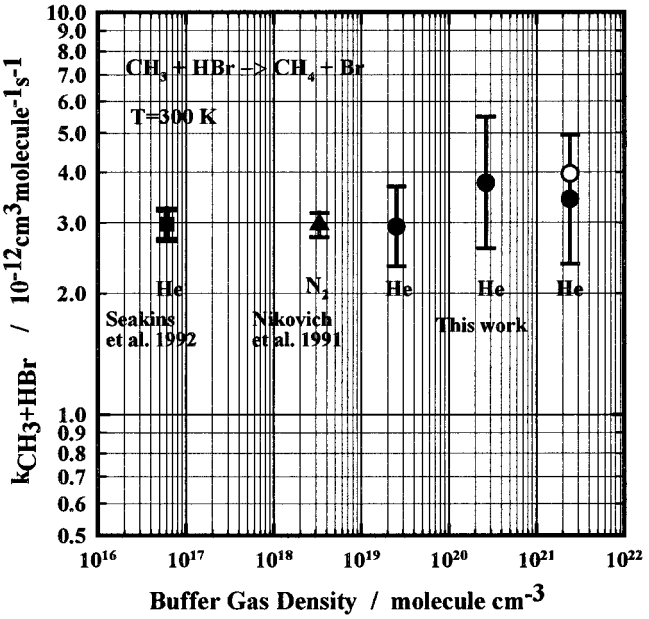

Figure 7. Rate constant of reaction 1 measured in the previous[18,21] and in the current work at different buffer gas densities.

indicates that there have been no interference from vibrationally excited radicals in these, previous, measurements.

Buffer Gas Density Dependence of the Rate Constant. Simple bimolecular metathesis reactions are generally believed to be independent of a buffer gas density. The discovery of negative apparent activation energies in a number of reaction of hydrocarbon free radicals with hydrogen halides and halogens may lead to reconsideration of this assumption.

An explanation of the negative activation energies for reactions that proceed via formation of an intermediate complex was given in terms of the RRKM theory.[20,23−25] The reaction products are separated from the intermediate complex by a transition state. It was shown that if the ground state energy of the transition state lies below the ground state of the reactants, and under the assumption of complete statistical energy redistribution in the intermediate complex, the statistical theories (such as RRKM) lead to prediction of a negative apparent activation energy for the reaction.[25] If this mechanism is responsible for the negative apparent activation energies experimentally observed, then a *buffer gas density dependence of the rate constant should be anticipated*.[25]

Theoretical calculations indeed found a weakly bounded complex in reactions of methyl radicals with hydrogen halides.[20] However, the calculated potential wells appeared to be rather shallow (1−3 kJ mol^{-1}), which makes the statistical assumption (fast energy redistribution due to the high density of energy levels in the intermediate complex) somewhat questionable. The theoretical calculations positioned the barriers of the transition states in reaction of methyl radical with hydrogen bromide above the ground-state energy of the reactants. To fit the experimental data, the authors were forced to adjust the transition state energies by ca. 3 kJ mol^{-1} down to reach an agreement with the experimental data and to obtain the negative apparent activation energy. However, the experimental rate constant of reaction 1 was then remeasured[18,21] and the revised value is a factor of 2 higher than that used in the theoretical work.[20]

The anticipated magnitude of the buffer gas density dependence strongly depends on the barrier energy. Being fitted to the corrected experimental value of the rate constant of reaction 1, statistical models (with the other parameters taken from the theoretical calculations[20]) predict an increase of the rate constant of reaction 1 of ca. 20−100% at high pressures. Our experimental measurement at both 10 and 100 bar He yielded systematically higher values of the rate constant by ca. 15−25% compared to these measured at low pressures (Figure 7). However, these deviations are still within the limits of the combined experimental and the model error. More accurate experimental measurements are required to establish the presence of the buffer gas density dependence of this reaction.

Appendix 1: The "Dead Volume Effect" in Preparation of Gas Mixtures

Typically, gas mixtures are prepared by sequential addition of gases to some (preliminarily evacuated) volume. The minor component is added first, the major component is added last. The composition is calculated based on the pressures measured after the addition of each component. The homogeneity of the mixture is provided either by allowing time long enough to ensure completion of the component diffusion, or by forced convection (caused by the flows of admixed gases or by stirring).

Forced convection is the only possibility to reduce the time required for mixture preparation. This is especially important for high-pressure mixtures, where the diffusion can easily take days or weeks.

Typically, any mixing volume has some narrow diameter parts attached (such as pressure gauges, valves and connecting tubings). Stirring (or convection induced by other means) in the main volume does not reach inside the volume associated with these parts. In the derivation below this volume is called the "dead volume." While the fraction of the dead volume is typically small, its effect on the mixture composition in the main volume is greatly enhanced when dilute mixtures are prepared (the "dead volume effect").

A brief derivation is given below.

A mixture of a gas A in gas M is prepared in a volume $V = V_1 + V_2$ (V_1, the "bulk" volume; V_2, the "dead volume") by addition of M to the volume initially filled by the gas A.

Efficient mixing in the bulk of the vessel during the gas addition is assumed (typically provided by the convection forced by the flow of gas M).

Notations. x_1, x_2, and x, mole fractions of A in V_1, V_2, and the overall mole fraction of A in the vessel; n_{A1}, n_{A2}, n_A, n_{M1}, n_{M2}, n_M, number of moles of A and M in V_1, V_2, and V (total), respectively; dn_M, an infinitesimal amount of M added.

Several Relations. $n_{A1} + n_{M1} = n_1$, total number of moles in V_1; $n_{A2} + n_{M2} = n_2$, total number of moles in V_2; $dn_1 = (1 - \beta)\, dn_M$, $dn_2 = \beta\, dn_M$, $\beta = V_2/(V_1 + V_2)$, the fraction of the dead volume; $\alpha = \beta/(1 - \beta) = V_2/V_1$, the ratio of the dead volume and the bulk volume of the vessel.

The mixture entering the dead volume at a given stage of preparation has the composition of the bulk volume mixture: $dn_{A2} = x_1 dn_2$.

Therefore, $dn_{A2} = (n_{A1}/(n_{A1} + n_{M1}))\, \beta\, dn_M$. Taking into account $n_{A1} = n_A - n_{A2}$, $dn_{A2} = -dn_{A1}$ (only M is added), one derives $dn_{A1} = -(n_{A1}/(n_{A1} + n_{M1}))\beta\, dn_M$. At any time, pressures in the "bulk" and the "dead volume" are equal, which infers $n_1/V_1 = n_2/V_2$, and, subsequently, nA1 + nM1 = (nA + nM)(1 − β).

After some transformations, one arrives at

$$dn_{A1}/n_{A1} = -\alpha\, dn_M/(n_A + n_M)$$

Integration of this equation with the initial conditions $n_M = 0$, $n_{A1} = n_A(1 - \beta)$ yields

$$x_1/x = x^{\alpha}$$

where $x_1 = n_{A1}/(n_{A1} + n_{M1})$, the mole fraction of A in the bulk volume, $x = n_A/(n_A + n_M)$, the overall (targeted) mole fraction (one obtained from the partial pressures), and $\alpha = V_2/V_1$ is the ratio of the dead volume and the bulk volume of the vessel.

Appendix 2: Transformation and Reduction of ODE System to a Dimensionless Form

A systematic procedure of reduction of a system of ordinary differential equations which describes a pulsed photolysis/transient absorption experiment to a dimensionless form and which automatically accounts for all absorptions before and after the photolytic pulse is outlined below.

The system of rate equations for a set of N elementary bimolecular reactions is written as follows:

$$dC_k/dt = \Sigma_{i \le j}\, \nu_{ijk}\, k_{ij}\, C_i C_j \quad k = 1, 2, 3, ..., N \qquad \text{(E7)}$$

The concentration of a species i, C_i, is divided into a permanent component, A_i, and a variable component, B_i. The permanent components exist before the photolysis, remain unchanged after the photolysis pulse, and are not changed during the secondary reactions. Variable components appear as a result of photolysis and secondary reactions. The initial amplitudes of the variable components are proportional to the laser pulse energy. The total concentration of a given chemical substance, C_i, is equal to the sum of permanent component, A_i, and the variable component, B_i; $C_i = A_i + B_i$

Taking into account $C_i = A_i + B_i$, A_i = constant, and the fact that the "permanent" components do not "react" with each other (the term A_iA_j disappears), the system of differential equations becomes

$$dB_k/dt = \Sigma_{i \le j}\, \nu_{ijk} k_{ij} B_i B_j + \Sigma_{i \le j}\, \nu_{ijk} k_{ij} (B_i A_j + A_i B_j) \qquad \text{(E8)}$$

Each variable component, B_i, can participate in a pseudo-first-order reaction with a permanent component A_j (rate constant k_{ij}) and in a bimolecular reaction with variable B_j (rate constant k_{ij}). The stoichiometric coefficients of kth species are ν_{ijk}. Only one contribution (B_iA_j or A_iB_j) can be nonzero in eq E8.

Only permanent components participate in the laser photolysis. The general stoichiometric equation for the photolysis is written as

$$0 = \Sigma_j \phi_{ij} A_j \qquad \text{(E9)}$$

where ϕ_{ij} is the quantum yield of the production of jth species in the photolysis of ith permanent species. The negative sign is assigned to the quantum yield of photodissociating molecule. The variable components after the pulse are

$$B_{j0} = F_1(\Sigma_i\, \sigma 1_i \phi_{ij} A_i) \qquad \text{(E10)}$$

where F_1 is the photon flux (photon/cm^2) of the photolytic light, and $\sigma 1_i$ is the absorption cross section of ith permanent species at the wavelength of the laser light.

Absorption of the monitoring light is characterized by the cross sections at the monitoring wavelength, $\sigma 2_i$. The variable component of the absorption of the monitoring light is described by the "absorption", Abs, the optical density with base e. There is a permanent absorption of the monitoring light, Abs_{00}, before and after the pulse ($t < 0$, $t > 0$) and variable absorption, Abs(t), after the pulse ($t > 0$),

$$Abs_{00} = (\Sigma_i\, \sigma 2_i A_i) L \qquad \text{(E11)}$$

$$Abs(t) = (\Sigma_i\, \sigma 2_i B_i) L \qquad \text{(E12)}$$

The amplitude of the variable absorption after the pulse is

$$Abs_0 = (\Sigma_i\, \sigma 2_i B_{i0}) L \qquad \text{(E13)}$$

B_{i0} is the ith variable component after the pulse, $\sigma 2_i$, is the absorption cross section of the ith species at the monitoring wavelength, and L is the optical path (cell) length.

For the sake of convenience in the numerical integration of the system of ordinary differential equations (E8) a dimensionless form is desirable. It could be done in a number of different ways. We choose the dimensionless form, which avoids using the laser energy flux or the radical concentration as fitting or input parameters. Instead, it employs initial absorption of one of the variable components as a fitting parameter and requires dimensionless combinations (such as ratios of rate constants, cross sections, and their combinations) as input parameters. Such

combinations are often directly derived from experimental data and have better accuracy than the individual rate constants or cross sections.

After normalization of all variable components to the initial concentration of one (the "reference") transient species (methyl radicals in our case) and introduction of dimensionless combinations, the ODE system becomes

$$dY_k/dt = \mathrm{Abs}_{CH_3,0} B \Sigma_{i\le j} \nu_{ijk} r_{ij} Y_i Y_j + \Sigma_{i\le j} \nu_{ijk} k_{ij} (Y_i A_j + A_i Y_j) \quad \text{(E14)}$$

The initial conditions are

$$Y_{k0} = B_{k0}/B_{CH_3,0} = (\Sigma_i \sigma 1_i \phi_{ik} A_i)/(\Sigma_i \sigma 1_i \phi_{i,CH_3} A_i) \quad \text{(E15)}$$

In this work, the "reference" concentration is the initial concentration of methyl radical. The dimensionless combinations are $Y_i = B_i/[CH_3]_0$, the normalized variable component of the ith species, $\mathrm{Abs}_{CH_3,0} = \sigma 2_{CH_3}[CH_3]_0 L$, the initial absorption of methyl radicals, $B = k_3/\sigma 2_{CH_3} L$, the combination of the recombination rate constant, absorption cross section, and the reactor length (which is directly measured in additional experiments), and $r_{ij} = k_{ij}/k_3$, the normalized rate constants of bimolecular reactions.

The set of differential equations (E14) together with the set of the initial conditions (E15) completes the formulation of the problem for numerical solution.

The specification of the initial conditions requires only the initial concentrations of the "permanent" species, their absorption cross sections for the laser light, and the quantum yields of the relevant photodissociation routes. No laser energy is required to fit the absorption kinetic curve, if the parameter B, the initial concentrations of the "permanent" species, and the ratios r_{ij} are known. The initial absorption of one of the free radicals (methyl in this case) is used as a fitting parameter. The absolute concentration of free radicals enters indirectly, via the initial absorption and the absorption cross sections.

The variable absorption and the intensity of the monitoring light are given by eqs E16 adn E17.

$$\mathrm{Abs}(t) = \mathrm{Abs}_{CH_3,0}(\Sigma_i (\sigma 2_i/\sigma 2_{CH_3}) Y_i) \quad \text{(E16)}$$

$$I(t) = I_0(t) \exp(-\mathrm{Abs}(t)) \quad \text{(E17)}$$

where $I_0(t)$ is the monitoring light intensity without the laser pulse entering the reactor. The absorption of the permanent species is *automatically accounted for* in eq E17.

Acknowledgment. This work was supported by the Separately Budgeted Research Support program at NJIT. Acknowledgment is made to the donors of the Petroleum Research Fund, administered by the American Chemical Society, for partial support of this research (Grant 31640-AC6).

References and Notes

(1) Andersen, H. C.; Kistiakowsky, G. B. *J. Chem. Phys*. **1943**, *11*, 6.
(2) Pritchard, H. O.; Pyke, J. B.; Trotman-Dickenson, A. F. *J. Am. Chem. Soc.* **1954**, *76*, 1201.
(3) Benson, S. W.; Buss, J. H. *J. Chem. Phys.* **1958**, *28*, 301.
(4) Fettis, G. C.; Trotman-Dickenson, A. F. *J. Chem. Soc.* **1961**, 3037.
(5) Hartley, D. B.; Benson, S. W. *J. Chem. Phys.* **1963**, *39*, 132.
(6) Rossi, M.; Golden, D. M. *J. Am. Chem. Soc.* **1979**, *101*, 1230.
(7) Tsang, W. *Int. J. Chem. Kinet.* **1978**, *10*, 821.
(8) Rossi, M. J.; Golden, D. M. *Int. J. Chem. Kinet.* **1983**, *15*, 1283.
(9) Tsang, W. *J. Am. Chem. Soc.* **1985**, *107*, 2872.
(10) Donaldson, D. J.; Leone, S. R. *J. Phys. Chem.* **1986**, *90*, 936.
(11) Jung, K.-H.; Choi, Y. S.; Yoo, H. S.; Tschuikow-Roux, E. *J. Phys. Chem.* **1986**, *90*, 1816.
(12) Russell, J. J.; Seetula, J. A.; Gutman, D. *J. Am. Chem. Soc.* **1988**, *110*, 3092.
(13) Russell, J. J.; Seetula, J. A.; Senkan, S. M.; Gutman, D. *Int. J. Chem. Kinet.* **1988**, *20*, 759.
(14) Russell, J. J.; Seetula, J. A.; Timonen, R. S.; Gutman, D.; Nava, D. F. *J. Am. Chem. Soc.* **1988**, *110*, 3084.
(15) Seetula, J. A.; Russell, J. J.; Gutman, D. *J. Am. Chem. Soc.* **1990**, *112*, 1347.
(16) Richards, P. D.; Ryther, R. J.; Weitz, E. *J. Phys. Chem.* **1990**, *94*, 3663.
(17) Seetula, J. A.; Gutman, D. *J. Phys. Chem.* **1990**, *94*, 7529.
(18) Nicovich, J. M.; Van Dijk, C. A.; Kreutter, K. D.; Wine, P. H. *J. Phys. Chem.* **1991**, *95*, 9890.
(19) Seakins, P. W.; Pilling, M. J. *J. Phys. Chem.* **1991**, *95*, 9874.
(20) Chen, Y.; Rauk, A.; Tschuikow-Roux, E. *J. Phys. Chem.* **1991**, *95*, 9900.
(21) Seakins, P. W.; Pilling, M. J.; Niiranen, J. T.; Gutman, D.; Krasnoperov, L. N. *J. Phys. Chem.* **1992**, *96*, 9847.
(22) Benson, S. W. *Thermochemical Kinetics*; Wiley: New York, 1976.
(23) McEwen, A. B.; Golden, D. M. *J. Mol. Struct*. **1990**, *224*, 357.
(24) Chen, Y.; Tschuikow-Roux, E. *J. Phys. Chem.* **1993**, *97*, 3742.
(25) Mozurkewich, M.; Benson, S. W. *J. Phys. Chem.* **1984**, *88*, 6429.
(26) Muller-Markgraf, W.; Rossi, M. J.; Golden, D. M. *J. Am. Chem. Soc.* **1989**, *111*, 956.
(27) Dobis, O.; Benson, S. W. *J. Am. Chem. Soc.* **1995**, *117*, 8171.
(28) Benson, S. W.; Dobis, O. *J. Phys. Chem. A* **1998**, *102*, 5175.
(29) Troe, J. *Ber. Bunsen-Ges. Phys. Chem*. **1969**, *73*, 906.
(30) Hippler, H.; Troe, J. *Ber. Bunsen-Ges. Phys. Chem*. **1971**, *75*, 27.
(31) Cobos, C. J.; Hippler, H.; Luther, K.; Ravishankara, A. R.; Troe, J. *J. Phys. Chem.* **1985**, *89*, 4332.
(32) Kaiser, E. W. *J. Phys. Chem.* **1993**, *97*, 11681.
(33) Allen, M. T.; Yetter, R. A.; Dryer, F. L. *Combust. Flame* **1997**, *109*, 449.
(34) Rohrig, M.; Petersen, E. L.; Davidson, D. F.; Hanson, R. K. *Int. J. Chem. Kinet.* **1996**, *28*, 599.
(35) Forster, R.; Frost, M.; Hamann, H. F.; Hippler, H.; Schlepegrel, A.; Troe, J. *J. Chem. Phys.* **1995**, *103*, 2949.
(36) Herzberg, G. *The Spectra and Structures of Small Free Radicals*; Cornell University Press: Ithaca, 1971.
(37) Van Den Berg, H. E.; Callear, A. B.; Norstrom, R. J. *Chem. Phys. Lett*. **1969**, *4*, 101.
(38) Basco, N.; James, D. G. L.; James, F. C. *Int. J. Chem. Kinet*. **1972**, *4*, 129.
(39) Bass, A. M.; Laufer, A. H. *Int. J. Chem. Kinet.* **1973**, *5*, 1053.
(40) Macperson M. T.; Pilling, M. J.; Smith, M. J. C. *J. Phys. Chem.* **1985**, *89*, 2268.
(41) *International Thermodynamic Tables of the Fluid State. Helium-4.* IUPAC Division of Physical Chemistry Commission on Thermodynamics and Thermochemistry Thermodynamic Tables Project; Angus, S., de Reuck, K. M., McCarty, R. D., Eds.; Pergamon Press: New York, 1977.
(42) Okabe, H. *Photochemistry of Small Molecules*; Wiley: New York, 1978.
(43) Huebert, B. J.; Martin, R. M. *J. Phys. Chem*. **1968**, *72*, 3046.
(44) Lightfoot, P. D.; Kirwan, S. P.; Pilling, M. J. *J. Phys. Chem.* **1988**, *92*, 4938.
(45) Donovan, R. J.; Hussain, D. *Trans. Faraday. Soc*. **1966**, *62*, 2643.
(46) Wight, C. A.; Leone, S. R. *J. Chem. Phys.* **1983**, *79*, 4823.
(47) Xu, Z.; Koplitz, B.; Wittig, C. *J. Phys. Chem*. **1988**, *92*, 5518.
(48) Johnson, R. O.; Perram, G. P.; Roh, W. B. *J. Chem. Phys*. **1996**, *104*, 7052.
(49) Hippler, H.; Luther, K.; Ravishankara, A. R.; Troe, J. *Z. Phys. Chem. (Munich)* **1984**, *142*, 1.
(50) Huebert, B. J.; Martin, R. M. *J. Phys. Chem.* **1968**, *72*, 3046.
(51) Robbins, D. E. *Geophys. Res. Lett.* **1976**, *3*, 213.
(52) Stewart, P. H.; Larson, C. W.; Golden, D. M. *Combust. Flame* **1989**, *75*, 25.
(53) Brouard, M.; MacPherson, M. T.; Pilling, M. J.; Tulloch, J. M.; Williamson, A. P. *Chem. Phys. Lett.* **1985**, *113*, 413.
(54) Stewart, P. H.; Smith, G. P.; Golden, D. M. *Int. J. Chem. Kinet.* **1989**, *21*, 923.
(55) Seakins, P. W.; Pilling, M. J. *J. Phys. Chem.* **1991**, *95*, 9878.
(56) Baulch, D. L.; Duxbury, J.; Grant, S. J.; Montague, D. C. *J. Phys. Chem. Ref. Data.* **1981**, *10* (Suppl. 1), 1-1.
(57) Baulch, D. L.; Cobos, C. J.; Cox, R. A.; Esser, C.; Frank, P.; Just, Th.; Kerr, J. A.; Pilling, M. J.; Troe, J.; Walker, R. W.; Warnatz, J. *J. Phys. Chem. Ref. Data* **1992**, *21*, 411.
(58) Parkes, D. A. *Chem. Phys. Lett.* **1981**, *77*, 527.

(59) Mellouki, A.; Talukdar, R. K.; Schmoltner, A.-M.; Gierczak, T.; Mills, M. J.; Solomon, S.; Ravishankara, A. R. *Geophys. Res. Lett*. **1992**, *19*, 2059.

(60) Hippler, H.; Otto, B.; Schroeder, J.; Schubert, V.; Troe, J. *Ber. Bunsen-Ges. Phys. Chem*. **1985**, *89*, 240.

(61) Reid, R. C.; Prausnitz, J. M.; Sherwood, T. K. *The Properties of Gases and Liquids*, 3rd ed.; McGraw-Hill: New York, 1977.

(62) Gardiner, W. C.; Troe, J. In *Combustion Chemistry;* Gardiner, W. C., Jr., Ed.; Springer-Verlag: New York, 1984; p 172.

(63) Callear, A. B.; Lambert, J. D. In *The Formation and Decay of Excited Species*; Comprehensive Chemical Kinetics, Vol. 3.; Bamford, C. H., Tipper, C. F. H., Eds.; Elsevier Publishing Company: New York, 1969.

(64) Jardley, J. T.; Fertig, M. N.; Moore, C. B. *J. Chem. Phys*. **1970**, *52*, 1450.

(65) Lambert, J. D.; Salter, R. *Proc. R. Soc*. **1957**, *A243*, 78.

(66) Baughcum, S. L.; Leone, S. R. *J. Chem. Phys.* **1980**, *72*, 6531.